Observing Brownian motion and measuring temperatures in vibration-fluidized granular matter

Patrick Mayor[1]**, Gianfranco D'Anna**[1]**, Alain Barrat**[2] **and Vittorio Loreto**[3]

[1] Institut de Physique de la Matière Complexe, Faculté des Sciences de Base, Ecole Polytechnique Fédérale de Lausanne, CH-1015 Lausanne, Switzerland
[2] Laboratoire de Physique Théorique, Unité Mixte de Recherche UMR 8627, Bâtiment 210, Université de Paris-Sud, 91405 Orsay Cedex, France
[3] Università degli Studi di Roma La Sapienza, Dipartimento di Fisica, and INFM, Center for Statistical Mechanics and Complexity, Piazzale A. Moro 5, 00185 Rome, Italy
E-mail: patrick.mayor@epfl.ch

Abstract. Understanding the behaviour of granular media, either at rest or moving under external driving, is a difficult task, although it is important and of very practical interest. Describing the motion of each individual grain is complicated, not only because of the large number of grains, but also because the mechanisms of interaction at the grain level involve complex contact forces. One would like to have, in fact, a description in terms of a few macroscopic quantities. Since a granular medium resembles a liquid or a gas when strongly vibrated or when flowing out of a container, a natural approach is to adopt usual equilibrium statistical mechanics tools in order to test if such a macroscopic description is possible. In other words, an interesting question is to investigate whether one can model granular media, when close to a liquid-like state for example, using viscosity, temperature, and so on, as one does for normal liquids. With this aim in view, we have developed a non-equilibrium version of the classical Brownian motion experiment. In particular, we have observed the motion of a torsion oscillator immersed in an externally vibrated granular medium of glass spheres, and have collected evidence that the motion is Brownian-like. An approximate fluctuation–dissipation relation holds, and we can define temperature-like and viscosity-like parameters.

Contents

1. Introduction

This work presents an experimental method devised to test standard equilibrium statistical mechanics results on vibrated granular matter. These concepts, notably the fluctuation–dissipation theorem [1], are well-known, and numerous experimental [2]–[6] and theoretical (see for instance [7]–[9] and references therein) studies have been carried out in order to investigate to what extent they are violated in systems far from equilibrium, or to propose possible generalizations in such complex situations.

In vibration-fluidized granular materials, like shaken sand, the assembly of particles featuring a large number of degrees of freedom interact by contact forces, and energy is continuously dissipated as grains collide into one another. Such a system is not in equilibrium in the thermodynamic sense, since the thermal energy $k_B T$ at room temperature is too small to produce any macroscopic grain rearrangement, and the fluctuation–dissipation theorem is therefore not expected to be valid. However, because of the sometimes liquid-like behaviour of granular matter [10], one can wonder how far the analogy can be pursued, namely how close such a system is to a 'thermal bath', exhibiting thermally induced Brownian motion. The outline of the paper is as follows. After briefly reviewing some basic concepts about the fluctuation–dissipation theorem (section 2), we describe the experimental setup in section 3. The main experimental findings concerning the validity of the fluctuation–dissipation theorem in vibrated granular media [5] are reviewed in section 4, and other studies, investigating the influence of the oscillator-bath interaction are then discussed in section 5. Finally, in section 6, we draw some preliminary conclusions.

2. The fluctuation–dissipation theorem

2.1. Langevin equation

The fluctuation–dissipation theorem finds its roots from the early theory made by Einstein [11, 12] to describe the irregular Brownian motion of particles suspended in a liquid [13]. It was first formulated in its modern form by Callen and Welton [1] by establishing a link between the fluctuations in a system at thermal equilibrium and the macroscopic response that is observed when an external perturbation is applied.

Let us consider the seemingly simple following situation: a one-dimensional harmonic oscillator, of mass m and stiffness K, is immersed into a fluid at temperature T. We suppose (Langevin hypothesis [14]) that the effect of this perturbing environment can be split into two parts: a viscous friction force, proportional to the oscillator velocity v (slowly varying contribution), and a random, fluctuating force $\xi(t)$ (rapidly varying contribution). Moreover, the latter part ξ is assumed to be a Gaussian white noise of zero mean; namely, it satisfies the following basic general properties:

$$\langle \xi(t) \rangle = 0 \qquad \text{and} \qquad \langle \xi(t)\xi(t') \rangle = q\delta(t - t'), \tag{1}$$

where $\langle \ldots \rangle$ denotes the statistical average over all possible realizations, and q is the amplitude of the random correlations, which will be related to simple parameters, such as the bath temperature, in the following.

The equation of motion for the oscillator position x thus reads

$$m\ddot{x}(t) + m\gamma\dot{x}(t) + m\omega_0^2 x(t) = \xi(t) + f_{\text{ext}}(t), \tag{2}$$

where γ is a parameter related to the viscosity of the system, $\omega_0 = \sqrt{K/m}$ is the natural angular frequency of the oscillator and f_{ext} denotes a possible other external force to which the system may be subjected.

2.2. Fluctuations (power spectral density S)

Let us first consider the situation where no external force is applied ($f_{\text{ext}} = 0$) and focus on the fluctuations of the oscillator around its equilibrium position due to its interaction with the bath. In that case, given the parameters $\Omega = \sqrt{\frac{1}{4}\gamma^2 - \omega_0^2}$ and $\lambda^{\pm} = \frac{\gamma}{2} \pm \Omega$, the solution of (2) with initial conditions $x(0) = x_0$ and $\dot{x}(0) = v_0$ reads

$$x(t) = x_h(t) + \frac{1}{2m\Omega} \int_0^t dt' \left(e^{-\lambda^-(t-t')} - e^{-\lambda^+(t-t')} \right) \xi(t'), \tag{3}$$

where $x_h(t) = Ae^{-\lambda^+ t} + Be^{-\lambda^- t}$ is the solution of the equation without the stochastic term $\xi(t)$, and A, B are constants depending on the initial conditions, given by $A = -(1/2\Omega)(v_0 + \lambda^- x_0)$, and $B = (1/2\Omega)(v_0 + \lambda^+ x_0)$.

Note that, even though Ω is complex when $\gamma < 2\omega_0$, the solution (3) is real in all cases. The time correlation function $G_{x_0 v_0}(t_1, t_2) = \langle x(t_1)x(t_2)\rangle_{x_0 v_0}$ can be calculated by using the solution (3)

and the conditions (1) to obtain

$$G_{x_0 v_0}(t_1, t_2) = x_h(t_1) x_h(t_2) + \frac{q}{4m^2\gamma\Omega^2} \left(\frac{\Omega}{\lambda^-} e^{-\lambda^-|t_1-t_2|} - \frac{\Omega}{\lambda^+} e^{-\lambda^+|t_1-t_2|} - \frac{\gamma}{2\lambda^-} e^{-\lambda^-(t_1+t_2)} \right.$$

$$\left. - \frac{\gamma}{2\lambda^+} e^{-\lambda^+(t_1+t_2)} + e^{-\lambda^- t_1 - \lambda^+ t_2} + e^{-\lambda^- t_2 - \lambda^+ t_1} \right). \tag{4}$$

Taking $t_1 = t_2 = t$ in the above result gives, in the limit $t \to \infty$ (stationary regime)

$$\langle x(t)^2 \rangle \xrightarrow{t \to \infty} \frac{q}{2m^2\gamma\omega_0^2}. \tag{5}$$

It is important to underline that the equipartition of energy principle $\frac{1}{2} K \langle x(t)^2 \rangle = \frac{1}{2} k_B T$ requires the amplitude q of the white noise correlations to be connected to the temperature T of the thermal bath according to the simple relation

$$q = 2m\gamma k_B T. \tag{6}$$

We notice that the time correlation function $G_{x_0 v_0}(t_1, t_2)$, as obtained in (4), still depends on x_0, v_0, through the term $x_h(t_1) x_h(t_2)$. It is possible to avoid this by assuming that these initial conditions are themselves distributed in accordance with the equipartition of energy:

$$\frac{1}{2} K \langle x_0^2 \rangle = \frac{1}{2} k_B T \qquad \text{and} \qquad \frac{1}{2} m \langle v_0^2 \rangle = \frac{1}{2} k_B T.$$

The deterministic term $x_h(t_1) x_h(t_2)$ can thus also be averaged over the initial conditions, which yields

$$\langle x_h(t_1) x_h(t_2) \rangle = \frac{k_B T}{2m\Omega^2} \left(\frac{\gamma}{2\lambda^-} e^{-\lambda^-(t_1+t_2)} + \frac{\gamma}{2\lambda^+} e^{-\lambda^+(t_1+t_2)} - e^{-\lambda^- t_1 - \lambda^+ t_2} - e^{-\lambda^- t_2 - \lambda^+ t_1} \right).$$

Using this averaged result in (4) shows that the two-time correlation function only depends on the time difference $t_1 - t_2$, thus exhibiting the stationary nature of the process: $G(t_1, t_2) = G(t_1 - t_2)$, with

$$G(t) = \frac{k_B T}{2m\Omega} \left(\frac{e^{-\lambda^-|t|}}{\lambda^-} - \frac{e^{-\lambda^+|t|}}{\lambda^+} \right). \tag{7}$$

A useful quantity is the power spectral density S, defined as twice the Fourier transform of the correlation function:

$$S(\omega) \equiv 2 \int_{-\infty}^{\infty} dt\, e^{-i\omega t}\, G(t) = \frac{4\gamma k_B T}{m \left[(\omega^2 - \omega_0^2)^2 + \gamma^2 \omega^2 \right]}. \tag{8}$$

2.3. Response function (susceptibility)

Let us study what happens when the system is subjected to an external force $f_{\text{ext}}(t)$. Focusing on large timescales compared to the typical relaxation time of the random force $\xi(t)$, we will

consider the deterministic equation (here, no bracket will be written and the use of the averaged quantities is implied)

$$m\ddot{x}(t) + m\gamma\dot{x}(t) + m\omega_0^2 x(t) = f_{\text{ext}}(t). \tag{9}$$

The linear response function $\chi(t)$, which gives information on how the system reacts to an externally applied perturbation, is defined as

$$x(t) = \int dt' \chi(t - t') f_{\text{ext}}(t'). \tag{10}$$

The validity of this linear relation implies that the external force should be small enough to guarantee that other terms involving powers of f_{ext} are negligible.

In the Fourier representation, this definition becomes $\tilde{x}(\omega) = \tilde{\chi}(\omega)\tilde{f}_{\text{ext}}(\omega)$. Therefore, writing (9) in the same representation immediately yields

$$\tilde{\chi}(\omega) = \frac{1}{m\left(\omega_0^2 - \omega^2 + i\gamma\omega\right)}. \tag{11}$$

2.4. Fluctuation–dissipation theorem

The two situations considered above are very different, the power spectral density S exhibits the fluctuations that the Brownian oscillator undergoes when it is left to move freely in a thermal bath. Logically, it is found in (8) that the fluctuations are proportional to the temperature of the bath.

On the other hand, the susceptibility χ gives information on the response to an external force, assumed to vary much more slowly than the rapid random force, which can be ignored in that case. The complex function (11) obtained can be split into a real and an imaginary part: we write $\tilde{\chi} = \tilde{\chi}' - i\tilde{\chi}''$, where in particular

$$\tilde{\chi}''(\omega) = \frac{\gamma\omega}{m\left[\left(\omega^2 - \omega_0^2\right)^2 + \gamma^2\omega^2\right]}. \tag{12}$$

Comparison of (8) and (12) shows very similar results, and there exists a simple relation between those very different concepts (fluctuation–dissipation theorem):

$$\frac{S(\omega)\,\omega}{4\tilde{\chi}''(\omega)} = k_B T. \tag{13}$$

It appears that the ratio on the left-hand side of (13) only depends on the temperature of the thermal bath, and is independent of other parameters such as the oscillator properties. It means that the complicated many-particle problem of the fluid molecules colliding with the oscillator can be described by few macroscopic parameters, such as the temperature and the viscosity.
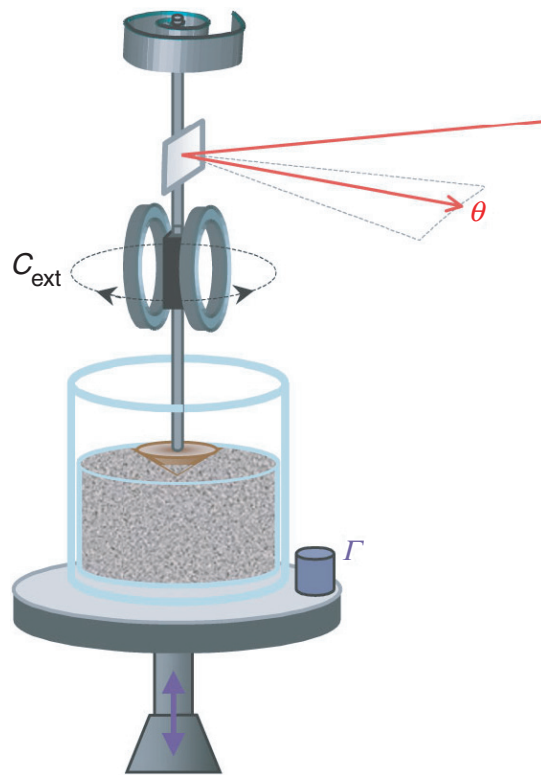
Figure 1. Sketch of the torsion oscillator immersed into the 'granular bath'. The granular medium, composed of glass beads of diameter $1.1 \pm 0.05\,\text{mm}$ is placed in a cylindrical container of height 60 mm and diameter 94 mm. An accelerometer measures the intensity of the external perturbations, Γ (see text for details). Notice that the oscillator cannot move in the vertical or horizontal directions.

3. Experiment

In order to investigate how much of this standard equilibrium formalism survives in shaken granular materials [5], the following experimental setup is used: a thin torsion oscillator, with moment of inertia I and elastic constant G, is immersed at some depth into the 'granular bath', made of millimetre-size glass beads (figure 1). Note the analogy with the situation described in [15] for a system at thermal equilibrium.

The container in which the beads are placed is continuously shaken by a vertical vibrator, with a high-frequency filtered white noise (cut off above 900 Hz and below 300 Hz in the experiments described). This vibration mode is chosen in order to ensure a homogeneous agitation and avoid undesired effects (such as pattern formation and convection rolls), which are observed when sinusoidal vibrations are used. It is not meant to provide a random torque with white noise spectrum to the oscillator; in any case, its motion is observed in a much lower frequency range than the vibrations applied (10–50 Hz, around the oscillator's natural frequency, where a useful signal can be measured).

The resulting vibrational intensity is quantified by an accelerometer fixed on the container, which measures the parameter Γ, defined as

$$\Gamma = \sqrt{\int A(f)\mathrm{d}f},\tag{14}$$

where $A(f)$ is the acceleration spectrum, normalized to the acceleration of gravity, and the integration is taken in the frequency range of about 1 Hz to 10 kHz.

For sinusoidal vibrations, $\Gamma = 1$ is the 'fluidization' threshold, above which a single grain starts to fly. Here, we typically use vibrational intensities between $\Gamma = 1$ and 15. The oscillator angular position θ is detected optically (see figure 1). For susceptibility measurements, two external coils and a permanent magnet fixed on the oscillator axis permit to apply a sinusoidal torque $C_{\mathrm{ext}}(t) = C_{\mathrm{e}}\sin(\omega t)$.

Note that if the experiment were performed in equilibrium conditions (with a plain liquid for example), the formalism developed in section 2 would be totally applicable to this situation. The Langevin equation (2) would then read as

$$I\ddot{\theta}(t) + \alpha\dot{\theta}(t) + G\theta(t) = R(t) + C_{\mathrm{ext}}(t),\tag{15}$$

where α is the friction coefficient and $R(t)$ is a random torque analogous to the random force $\xi(t)$ introduced in section 2. The corresponding expressions (8) and (11) for $S(\omega)$ and $\tilde{\chi}(\omega)$ would be adapted as follows:

$$S(\omega) \equiv 2\int \mathrm{d}t e^{-\mathrm{i}\omega t}\langle\theta(t)\theta(0)\rangle = \frac{4\alpha k_B T}{I^2\left(\omega^2 - \omega_0^2\right)^2 + \alpha^2\omega^2}$$

and

$$\tilde{\chi}(\omega) \equiv \frac{\tilde{\theta}(\omega)}{\tilde{C}_{\mathrm{ext}}(\omega)} = \frac{1}{I\left(\omega_0^2 - \omega^2\right) + \mathrm{i}\alpha\omega},$$

where $\tilde{\theta}(\omega)$ and $\tilde{C}_{\mathrm{ext}}(\omega)$ are the Fourier transforms of $\theta(t)$ and $C_{\mathrm{ext}}(t)$, respectively.

4. Test of the equilibrium formalism

Analysis of the angular deflection time-series $\theta(t)$ in the free mode ($C_{\mathrm{ext}} = 0$) provides the noise power spectral density $S(\omega)$, shown in figure 2(a) for different values of Γ. On the other hand, using the oscillator in forced mode (with an externally applied torque $C_{\mathrm{ext}}(t)$) gives the complex susceptibility $\tilde{\chi}(\omega)$, whose modulus $|\tilde{\chi}(\omega)|$ is shown in figure 2(b). The amplitude of the external torque is small enough to be in the regime of linear response.

It appears that $|\tilde{\chi}(\omega)|$ is fitted remarkably well by the standard expression for the damped oscillator:

$$|\tilde{\chi}(\omega)| = \frac{1}{\sqrt{I^2\left(\omega_0^2 - \omega^2\right)^2 + \alpha^2\omega^2}}.\tag{16}$$

This reveals that the Langevin equation of motion (15) describes well the linear response of the immersed oscillator, and allows us to extract a granular friction coefficient α, or a granular
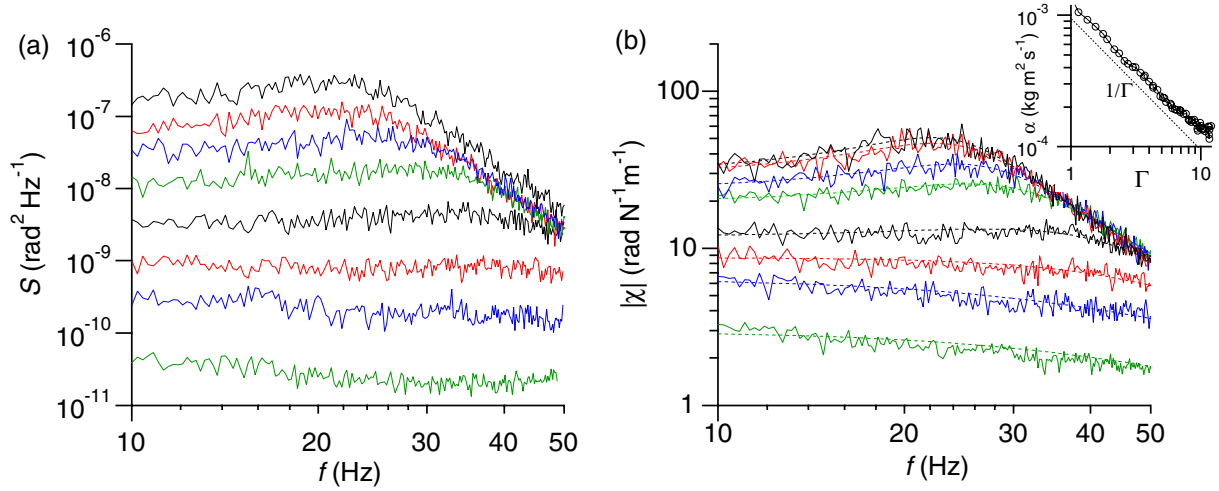
Figure 2. Power spectral density (a) and modulus of the complex susceptibility (b) versus the frequency, $f = \omega/2\pi$, for different vibrational intensities Γ: from top to bottom, 11.6, 10.0, 7.3, 5.4, 3.7, 2.2, 1.5 and 1.0. Results obtained with a conical probe of apex angle $120°$, covered with a single layer of glass beads, glued on by epoxy adhesive. The probe is immersed to about 11 mm from the granular surface. The vibration consists of a high-frequency filtered white noise, cut off below 300 Hz and above 900 Hz. In (b), each curve is fitted (dashed line) with its corresponding equilibrium expression (see text for details). The moment of inertia of the oscillator is $I = 1.5 \times 10^{-6}\,\mathrm{kg\,m^2}$, and the applied torque amplitude is $C_\mathrm{e} = 3.2 \times 10^{-5}\,\mathrm{N\,m}$. Inset: friction coefficient α, obtained from the fit to the curves $|\tilde{\chi}(\omega)|$, versus Γ. The dotted line is a power law $\alpha \propto 1/\Gamma$. This $1/\Gamma$ dependence is also systematically observed using susceptibility data obtained with probes of different shapes, as discussed later.

viscosity $\mu \propto \alpha$. From the fitting parameters at different Γ, we observe that $\alpha \propto 1/\Gamma$ (see inset of figure 2(b)).

Moreover, the previous data allow to calculate the fluctuation–dissipation ratios $S(\omega)\omega/(4\tilde{\chi}''(\omega))$, which are shown in figure 3(a). The ratios, even though not constant, are surprisingly 'flat', especially compared to what has been measured in other non-equilibrium thermal systems, such as in glycerol [2] and laponite [3].

This means that the high-frequency driven agitation of the granular medium acts on the oscillator as a source of random torque with white spectrum, at least in the 10–50 Hz range under consideration. Energy is thus injected at high frequency, and spreads into a low-frequency white spectrum.

Since those ratios do not exhibit a strong frequency dependence, this provides support for the existence of a fluctuation–dissipation relation in off-equilibrium driven granular steady states. The theorem can thus be used to define an effective temperature, T_eff. Figure 3(b) shows the averaged fluctuation–dissipation ratio levels, that is, $k_B T_\mathrm{eff}$, versus Γ (black curve). On fitting to a power law, we obtain $k_B T_\mathrm{eff} \propto \Gamma^p$ with p close to 2, thus giving $T_\mathrm{eff} \propto \Gamma^2$.

This is only a first-order approximation: close inspection of figure 3(a) reveals indeed a small frequency dependence. However, a useful torsion signal is only detected around the oscillator
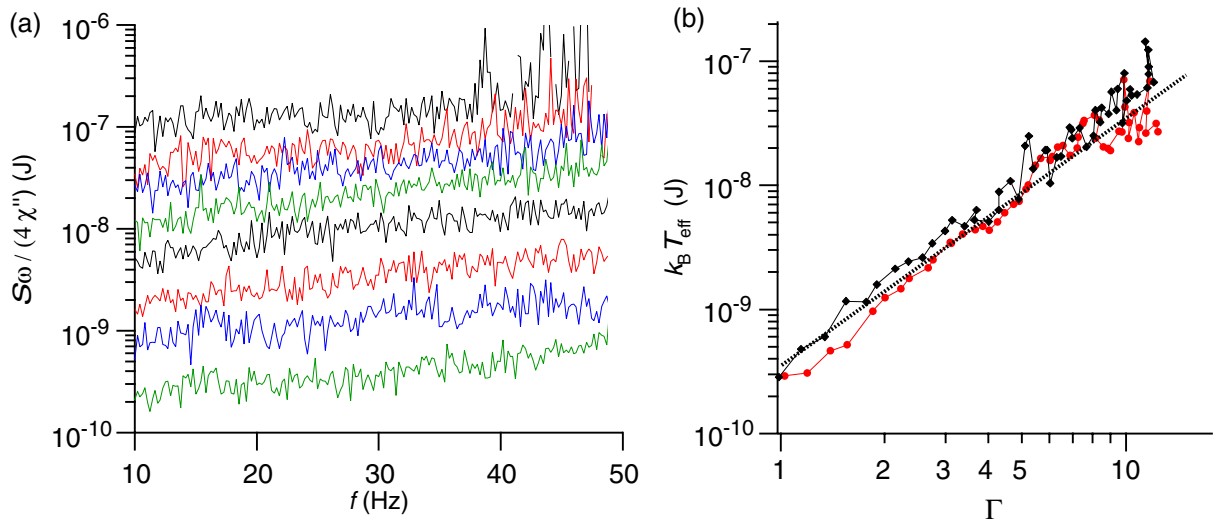
Figure 3. (a) Fluctuation–dissipation ratios $S(\omega)\omega/(4\tilde{\chi}''(\omega))$ versus the frequency $f = \omega/2\pi$ for different vibrational intensities Γ: from top to bottom, 11.6, 10.0, 7.3, 5.4, 3.7, 2.2, 1.5 and 1.0. (b) Effective temperature versus vibrational intensity Γ, as obtained from fluctuation–dissipation levels in (a) averaged between 10 and 50 Hz (black symbols), and from experiment using a conical probe with triple moment of inertia (red symbols). A power law fitted to the data gives $T_{\text{eff}} \propto \Gamma^p$, with $p = 2.1$. The dashed line has equation $k_B T_{\text{eff}} = 3.5 \times 10^{-10}\,\Gamma^2$.

eigenfrequency, limiting the accessible frequency range. In the frame of this approximation, our results suggest that due to the complex dissipation processes between the grains only a fixed fraction of the energy injected by the vibrator is effectively available as granular kinetic energy and is 'sensed' by the oscillator.

In fact, we notice that the order of magnitude of the thermal energy $k_B T_{\text{eff}}$, as measured here, is consistent with realistic values of the mean kinetic energy per particle, as measured by grain-tracking methods [16, 17]. Thus, the effective temperature T_{eff} measured seems to be related to the granular temperature, as usually defined in granular gases [18, 19].

5. Changing the 'thermometer' properties

This section is devoted to the presentation of results addressing the dependence of T_{eff} on the oscillator properties.

5.1. Influence of the moment of inertia

By fixing a cylindrical weight on the probe axis above the granular surface, it is possible to vary the moment of inertia I of the oscillator without otherwise modifying its geometrical properties. By changing this parameter, we obtain different susceptibilities, and different power spectral densities as well (as expected from the formulas for $\tilde{\chi}(\omega)$ and $S(\omega)$ introduced above).
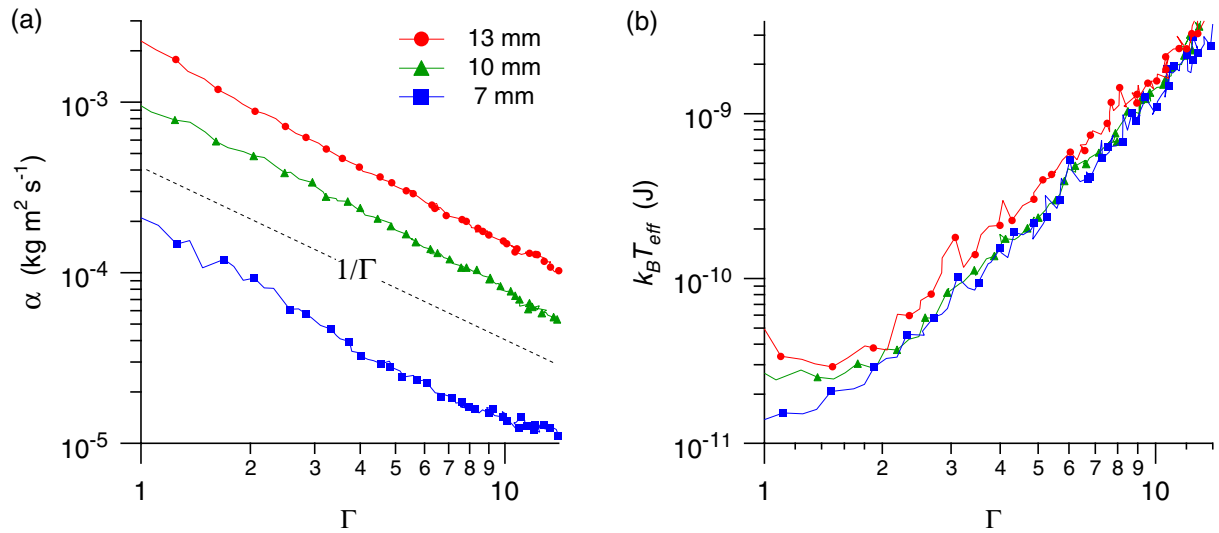
Figure 4. (a) Friction coefficient α for cylindrical probes of different diameters and smooth surfaces, obtained from the fits to the curves $|\tilde{\chi}(\omega)|$, versus Γ. The diameters are 13 mm (red curve), 10 mm (green curve) and 7 mm (blue curve). The dotted line is a power law $\alpha \propto 1/\Gamma$. The immersion depth is about 20 mm. (b) Effective temperature T_{eff} versus Γ. Notice the deviation from the $T_{\text{eff}} \propto \Gamma^2$ dependence at low Γ (see text for details). On both graphs, for clarity, only one symbol for every three data values is marked.

However, we notice that the fluctuation–dissipation ratios exhibit very little variation when I is modified. Data obtained using conical probes with different moments of inertia are presented in figure 3(b). The effective temperature measured seems to be almost independent of this parameter.

5.2. Influence of the probe shape

Experiments made with cylindrical probes of different diameters reveal interesting features. First of all, the susceptibility and power spectral density are very different depending on the probe used: they exhibit a distinct peak for small diameters, which tends to flatten and disappear for bigger diameters (at similar Γ). The fact that damping is more important for bigger probes is clear in figure 4(a), which shows the friction coefficient α versus Γ for cylindrical probes of different diameters.

However, even though these different friction characteristics yield very different susceptibilities and power spectral densities, the probe diameter seems to have little influence on the effective temperature T_{eff}, as shown in figure 4(b).

Notice that a deviation from the $T_{\text{eff}} \propto \Gamma^2$ dependence is seen close to the fluidization threshold $\Gamma \approx 1$. The main reason is that the oscillator, which cannot move in the vertical or horizontal directions, becomes a source of localized vibration at low Γ and therefore 'heats' the granular medium around the probe. Logically, we observe that this phenomenon is more pronounced with the bigger probes. Because of these observations, the study of the granular dynamics for $\Gamma < 1$, in the so-called granular glass, requires a different approach [20, 21].
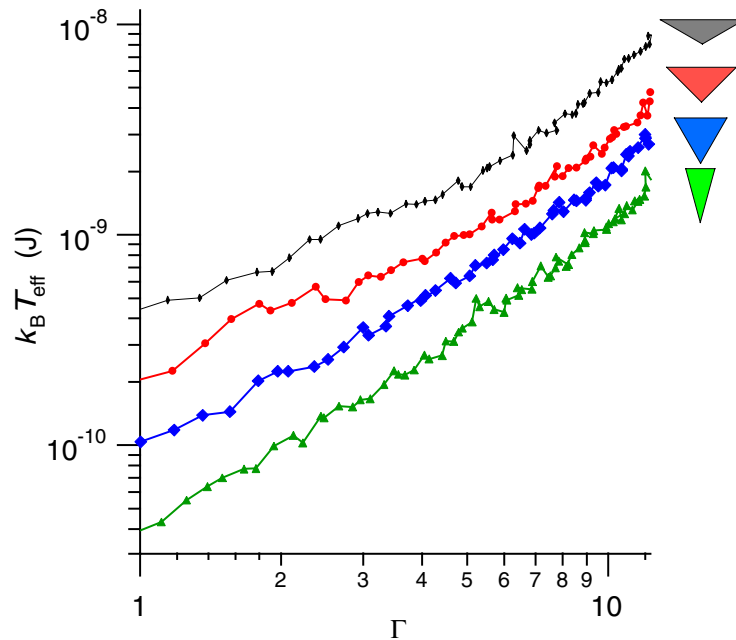
Figure 5. Effective temperature T_{eff} versus Γ, obtained with conical probes of different apex angles. The cones are smooth (not covered with a layer of beads) and the apex angles are, from top to bottom, 120, 90, 60 and 30°. The probes are immersed at a depth of 20 mm from the granular surface.

However, there exists a difference between T_{eff} measured by conical and cylindrical probes. Data obtained using conical probes with different apex angles are shown in figure 5 (note that cones used here are smooth—the effect of the surface roughness is discussed below). These results show that the effective temperature measured is smaller for narrower cones and increases with the apex angle.

This effect is probably related to the intrinsic anisotropy of the system under gravity. Although the diameter of the horizontal section of the probe has little effect on T_{eff}, the angle of inclination of the surface exposed to the granular agitation, with respect to the vertical axis, seems to be a relevant parameter. The granular temperature is anisotropic [17], corresponding to vertical and horizontal impulse components. One thus expects in particular the transfer of the vertical impulse into torsion momentum to depend on the geometry and the surface state of the probe.

5.3. Influence of the probe section

Here we consider probes whose main lateral surface is vertical, like cylinders, and study the influence of the horizontal section. Those issues are represented in figure 6. For comparison, we also include the previously obtained results with smooth cylinders.

It appears that probes that have a more complicated profile tend to give higher values of the effective temperature. T_{eff} increases when the probe 'grips' the granular medium better.

Another observation can be made from figure 6: while the data corresponding to the smooth cylinders (blue curves in figure 6) exhibit a precise $T_{eff} \propto \Gamma^2$ behaviour, the other results obtained
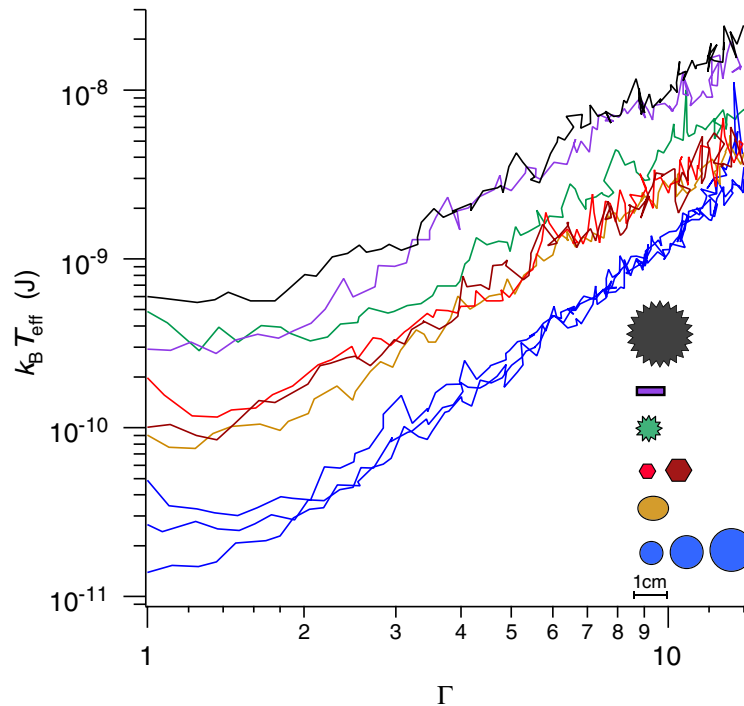
Figure 6. Effective temperature T_{eff} versus Γ, obtained using different probes with vertical lateral surfaces. The probe sections vary, as sketched on the graph. From top to bottom: outer diameter 22 mm with 24 teeth, about 1.2 mm high (black curve); rectangular section 2 mm × 8 mm (purple curve); outer diameter 8 mm, with 12 teeth, about 1 mm high (green curve); hexagons with biggest diameters 5 mm (red curve) and 8 mm (dark red curve); ellipse with axes 9 and 7 mm (yellow curve). We also include the results obtained with cylinders of diameters 7, 10 and 13 mm (blue curves) already shown in figure 4(b). All probes are immersed at a depth of 20 mm from the granular surface.

with 'rougher' probes tend to correspond to an exponent slightly lower than 2 (this phenomenon also occurs in figure 5). This is possibly due to the fact that, as already mentioned, rougher probes are more likely to locally fluidize the granular bath around them, and therefore maintain higher temperature values. Note that by 'roughness' we mean surface irregularities or features in the probe section with lengths of the same order as the size of the grains (we do not change the surface roughness at the atomic scale here).

Another aspect needs to be underlined: the curves $|\tilde{\chi}(\omega)|$ and $S(\omega)$, obtained using probes with rough surface, tend to exhibit a shift of the peak towards high frequencies as the damping increases. This behaviour is shown for $|\tilde{\chi}(\omega)|$ in figure 7. We notice that, while, for a smooth cylinder, the susceptibility peak does not shift significantly, it moves drastically to the right as Γ decreases for a cylinder with a layer of beads glued on its surface. (The same phenomenon can be observed for power spectral density measurements.)

The susceptibility modulus, according to its equilibrium expression (16), reaches a maximum at the resonant angular frequency

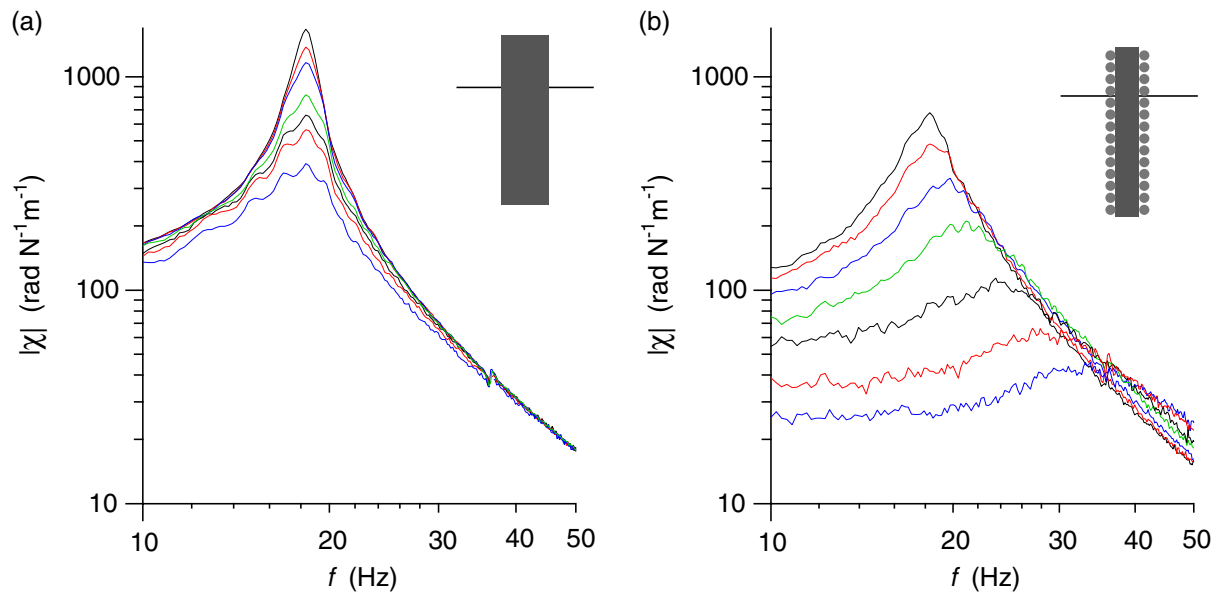$$\omega_{max} = \sqrt{\omega_0^2 - \frac{\alpha^2}{2I^2}}.$$

Figure 7. Modulus of the complex susceptibility versus the frequency, $f = \omega/2\pi$, for different vibrational intensities Γ. From top to bottom, on both graphs: $\Gamma = 11.9, 8.7, 6.7, 4.1, 2.8, 1.8$ and 1.0. (a) Measurements made using a smooth cylinder of diameter 5 mm. (b) Measurements made using a thin cylinder with a single layer of glass beads glued on its surface, outer diameter $\sim$5 mm. Both probes are immersed at a depth $L = 20$ mm.

Since α is inversely proportional to Γ, the resonant frequency should actually decrease when the damping increases. This is verified for smooth cylinders (it requires more important damping than that observed in figure 7(a)), but obviously not for rough probes, which thus seem to exhibit an apparent increase of the elastic constant G.

Actually, when the probe surface is not smooth, two grain-level mechanisms can be involved and must be considered here:

(i) The jutting probe features are likely to be sources of a network of grain-chains that resist the rotation of the oscillator, thus effectively increasing its stiffening. This network is expected to be stronger as the vibrations get weaker.

(ii) While rotating a cylinder with smooth surface can be done in principle without changing the total volume of the granular medium, to rotate a cylinder with 'rough' section, for instance involving teeth or a layer of glued grains, requires an increase of the total volume of the granular medium (dilatancy). This geometrical barrier against rotation can effectively increase the stiffness of the torsion oscillator. At high applied torque, or when the vibrational intensity is weak, this geometrical dilatancy causes local fluidization around the probe.

5.4. Influence of the immersion depth

Figure 8 shows the effective temperature measured as a function of the immersion depth L of the oscillator, for different probes. The data obtained for very shallow immersions are not given.
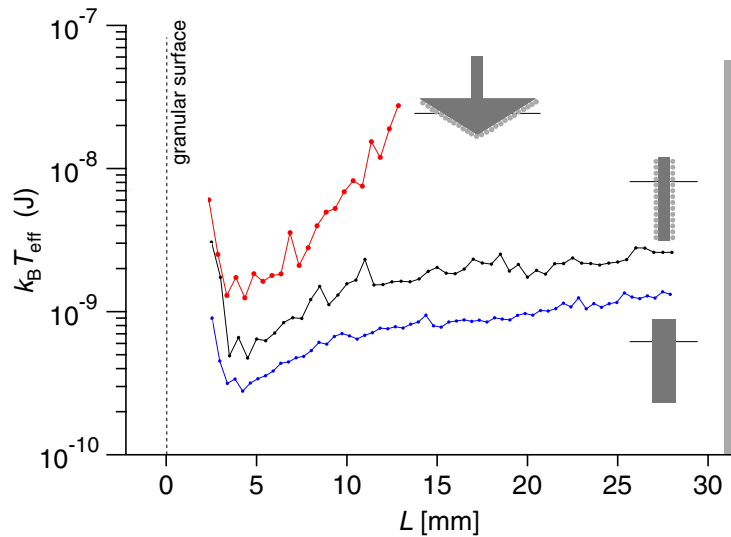
Institute *of* **Physics** 🔶 DEUTSCHE PHYSIKALISCHE GESELLSCHAFT

Figure 8. Effective temperature T_{eff} at $\Gamma = 9$ versus the immersion depth of the oscillator, L, for different probes: conical, with a single layer of glass beads (red curve); cylindrical, with a single layer of glass beads, outer diameter 7 mm (black curve); cylindrical with smooth surface, diameter 7 mm (blue curve). Notice that the precise position of the surface is unknown for a vibrated granular medium, but is approximately at $L = 0$ (vertical dashed line). The bottom of the container is at $L = 31$ mm (grey rectangle). We also note that, owing to boundary effects, in the layer close to the surface (about $0 < L < 5$ mm), the fluctuation–dissipation ratio is no longer flat and we do not extract an effective temperature in this region.

Indeed, we observe that in a layer close to the surface, the measured fluctuation–dissipation ratios exhibit a strong frequency dependence, and they become 'flat' only at sufficient immersion depth (approximately at the depth where a minimum appears in the curves of figure 8).

Underneath this surface layer, we notice that the effective temperature T_{eff} increases with the depth L. This is possibly related to the fact that the source of vibrations is the bottom of the container, and thus the temperature gets higher as we approach the 'hot' plate. It also suggests that the density of the granular medium slightly decreases with the depth, as observed in simulations [22] and measurements [23] (except possibly the surface layer, where we found no evidence of the fluctuation–dissipation ratios being constant).

5.5. Discussion

In this section, we have considered to what extent the oscillator type, as well as its immersion depth, influences the effective temperature T_{eff} measured. Firstly, it appears that T_{eff} is independent of the moment of inertia of the probe, if all other characteristics are fixed. Then, we noticed that T_{eff} does not depend on the diameter of cylindrical probes either. However, we have also observed that T_{eff} had the tendency to take higher values when the probe is immersed deeper into the granular material, or when cones with wider apex angles are used, or when the probe surface is 'rougher'. All these results seem to indicate that the more the oscillator can interact with the granular medium, the higher the effective temperature is.

In fact, it is worth mentioning that the oscillator formally conforms to the standard equilibrium formalism only for 'smooth' probes, that is, when there are no features or irregularities in the section with characteristics lengths of the same order as the grain size. In that case, the classical Langevin equation of motion (2), for an oscillator immersed in a thermal fluid, also seems to be a correct description for the oscillator immersed in a shaken granular medium.

On the other hand, when such irregularities are present, the response of the oscillator is more complex: as mentioned previously, effects occuring at the grain-level have to be considered, such as the geometrical dilatancy and the development of a network of grain chains resisting the probe rotation. In such a case, the equation of motion for the oscillator is expected to involve 'non-classical' terms, related to these effects. This unknown equation of motion should reproduce in particular the apparent increase of the elastic modulus observed in figure 7(b).

Similar grain-level related effects may also be invoked when the probe immersion depth is of the same order as the dimension of the grains (figure 8). Also in this case, when the probe immersion depth is only a few grain layers, the classical equation of motion does not capture all the phenomenon that is actually occurring. This is not surprising: in fact, similar problems would appear if we tried to describe the classical experiment by using an 'atomic scale' probe.

6. Conclusion

In this paper, we have reviewed some recent experimental results aimed at checking the validity of the fluctuation–dissipation theorem in vibrated granular matter [5]. The main finding reported here consists in the possibility to separate slow and fast degrees of freedom in vibration-fluidized granular media and thus to model the many-particle problem with a simple Langevin equation involving two instrinsic parameters: an effective friction coefficient α and an effective temperature T_{eff}.

In this framework, the oscillator behaves indeed as a Brownian particle, and driven granular matter can be seen as a macroscopic 'thermal bath'. We note that the analogy is only formal, since the granular medium is never in equilibrium in the thermodynamic sense. The experiments also reveal that this simple picture is only valid up to a certain extent. Mechanical and rheological properties, as well as anisotropy and inhomogeneity effects due to gravitation, play an important role in the specification and the measurement of thermodynamical-like properties [24], inducing differences and complications that do not occur in 'plain' fluids made of atoms. This is particularly obvious when the response involves grain level phenomena, as discussed above. These phenomena are triggered as soon as the interaction between the probe and the granular medium takes place on length scales that are comparable to the grain dimension. When these complications are not present, notably with appropriate probe sections and surfaces, the formal analogy to the classical Brownian motion experiment in equilibrium systems is surprisingly good.

In future work, more experiments will be required to elucidate the role of the different parameters specifying a granular medium and its interactions with the measuring devices, also at the atomic scale, notably to investigate how the friction affects the effective temperature.

References

[1] Callen H B and Welton T A 1951 Irreversibility and generalized noise *Phys. Rev.* **83** 34–40

[2] Grigera T S and Israeloff N F 1999 Observation of a fluctuation–dissipation-theorem violation in a structural glass *Phys. Rev. Lett.* **83** 5038–41

[3] Bellon L, Ciliberto S and Laroche C 2001 Violation of the fluctuation–dissipation relation during the formation of a colloidal glass *Europhys. Lett.* **53** 511–7

[4] Hérisson D and Ocio M 2002 Fluctuation-dissipation ratio of a spin glass in the aging regime *Phys. Rev. Lett.* **88** 257202

[5] D'Anna G, Mayor P, Barrat A, Loreto V and Nori F 2003 Observing Brownian motion in vibration-fluidized granular matter *Nature* **424** 909–12

[6] Abou B and Gallet F 2004 Probing a nonequilibrium Einstein relation in an aging colloidal glass *Preprint* cond-mat/0403561

[7] Cugliandolo L and Kurchan J 1993 Analytical solution of the off-equilibrium dynamics of a long-range spin-glass model *Phys. Rev. Lett.* **71** 173–6

[8] Cugliandolo L, Kurchan J and Peliti L 1997 Energy flow, partial equilibration and effective temperatures in systems with slow dynamics *Phys. Rev.* E **55** 3898–914

[9] Crisanti A and Ritort F 2003 Violation of the fluctuation–dissipation theorem in glassy systems: basic notions and the numerical evidence *J. Phys. A: Math. Gen.* **36** R181–R290

[10] Jaeger H M, Nagel S R and Behringer R P 1996 Granular solids, liquids and gases *Rev. Mod. Phys.* **68** 1259–73

[11] Einstein A 1905 Über die von der molekularkinetischen Theorie der Wärme geforderte Bewegung von in ruhenden Flüssigkeiten suspendierten Teilchen *Ann. Physik* **17** 549–60

[12] Einstein A 1906 Zur Theorie der Brownschen Bewegung *Ann. Physik* **19** 371–81

[13] Brown R 1828 A brief account of microscopical observations made in the months of June, July, and August, 1827, on the particles contained in the pollen of plants; and on the general existence of active molecules in organic and inorganic bodies *Phil. Mag.* **4** 161–73

[14] Langevin P 1908 Sur la théorie du mouvement brownien *C. R. Acad. Sci. Paris* **146** 530–3

[15] Uhlenbeck G E and Goudsmit S 1929 A problem in Brownian motion *Phys. Rev.* **34** 145–51

[16] Dixon P K and Durian D J 2003 Speckle visibility spectroscopy and variable granular fluidization *Phys. Rev. Lett.* **90** 184302

[17] Yang X, Huan C, Candela D, Mair R W and Walsworth R L 2002 Measurements of grain motion in dense, three-dimensional granular fluid *Phys. Rev. Lett.* **88** 044301

[18] Puglisi A, Baldassarri A and Loreto V 2002 Fluctuation-dissipation relations in 2D driven granular gases *Phys. Rev.* E **66** 061305

[19] Barrat A, Loreto V and Puglisi A 2004 Temperature probes in binary granular gases *Physica* A **101** 513–23

[20] D'Anna G and Gremaud G 2001 Vogel–Fulcher–Tammann-type diffusive slowdown in weakly perturbed granular media *Phys. Rev. Lett.* **87** 254–302

[21] D'Anna G, Mayor P, Gremaud G, Barrat A and Loreto V 2003 Extreme events-driven glassy behavior in granular media *Europhys. Lett.* **61** 60–6

[22] Barrat A and Loreto V 2000 Response properties in a model for granular matter *J. Phys. A: Math. Gen.* **33** 4401–26

[23] Philippe P and Bideau D 2002 Compaction dynamics of a granular medium under vertical tapping *Europhys. Lett.* **60** 677–83

[24] A vast amount of literature on this subject has been inspired by the pioneering work by S F Edwards, see: Edwards S F 1994 *Granular matter: An Interdisciplinary Approach* ed A Mehta (Berlin: Springer)